Dopaminergic Neurons in the Brain Orchestrates Cardiac and Behavioral Threat Responses

Masato Tsuji[1, *], Daisuke Jinkoma[1], Yuki Uemura[1], Ayako Ogasawara[1], and Kazuo Emoto[1, 2, *]

[1]Department of Biological Sciences, Graduate School of Science

[2]International Research Center for Neurointelligence (WPI-IRCN), The University of Tokyo, 7-3-1 Hongo, Bunkyo-ku, Tokyo, 113-0033, Japan

[*]Correspondence: mtsuji@bs.s.u-tokyo.ac.jp; emoto@bs.s.u-tokyo.ac.jp

TEL: +81-3- 5841-4426 FAX: +81-3- 5841-4632

Key words: Heart, Threat, Dopamine, Drosophila, Interoception

ABSTRACT

Heartbeat and behavior are often modulated in a tightly coupled fashion, which is believed advantageous for survival. For instance, when threatened animals show freezing or escaping, the brain drives cardiac deceleration or acceleration, respectively. In turn, the heart sends ascending feedback to the brain, but whether and how the descending regulation of and the ascending feedback from the heart might drive the heart-behavior coupling remains unknown. Here we show in Drosophila that mechanical threat induces not only locomotion but cardiac deceleration. We further identified two pairs of dopaminergic neurons in the brain, called DA-WED neurons, that are responsible for threat-induced cardiac deceleration. Silencing DA-WED neurons suppresses threat-induced cardiac deceleration, while activation of DA-WED neurons can replace threat to induce cardiac deceleration. Our calcium imaging analysis shows that threat activates DA-WED neurons. Interestingly, silencing DA-WED neurons to block threat-induced cardiac deceleration reduces locomotion. Conversely, direct manipulation of cardiomyocytes to artificially induce cardiac deceleration promotes locomotion. Together, our data reveals a neuronal mechanism in which mechanical threat regulates the heartbeat through dopaminergic neurons in the brain, and suggests how these neurons possibly prompt feedback from the heart to modulate behavior.

INTRODUCTION

Heartbeat modulation is thought to play significant roles in successful execution of behavior. Threatened animals, for instance, typically show freezing or escape behavior that are accompanied by cardiac deceleration and acceleration, respectively[1]. Such a tight coupling of the behavior and the heartbeat is potentially advantageous for survival: cardiac deceleration might minimize the brain-wide representation of the heartbeat[2–5] to sharpen the sensory processing in the brain[16], while cardiac acceleration boosts the supply of energy source to the muscles[7].

In mammals, heartbeat is governed by sympathetic and parasympathetic branches of the autonomic nervous system (ANS) that innervate the heart[7–15]. The sympathetic nervous system originates from the nucleus tractus solitarius (NTS) in the brain and projects through multiple synapses to the heart, accelerating the heartbeat[7]. On the other hand, the parasympathetic nervous system originates from the dorsal motor nucleus of the vagus nerve and nucleus ambiguus, and projects directly to the heart[16,17], decelerating the heartbeat[7,16]. Antagonistic actions of sympathetic and parasympathetic nervous systems appear to be mediated both by norepinephrine/acetylcholine receptors in cardiomyocytes and by intracardiac nervous system[18–22].

Such an ANS-based mechanism is engaged in threatened animals by the so-called fear circuitry in the brain[23–25], typically producing cardiac deceleration followed by acceleration[1,26–31]. Circuit-wise, the periaqueductal gray (PAG) is considered the output hub of the fear circuitry and modulates the heartbeat through the hypothalamus, midbrain, pons, and medulla oblongata[32]. In addition, hypothalamic nuclei such as the

dorsomedial hypothalamus (DMH)[33] and the arcuate nucleus (ARC), as well as the anterior cingulate cortex (ACC)[34], also modulate the heartbeat upon threats[35–41].

In contrast to the descending regulation of the heartbeat described above, how it is coupled to behavior is much less known. In this regard, feedback from the heart to the brain is increasingly attracting attention. Such a brain function to receive inputs from peripheral organ is often called interoception[42]. In particular, cardiac interoception is mediated by an array of sensory neurons innervating the heart and aortic arch, contained in either the parasympathetic nervous system or forming distinct circuits emanating from the spinal cord dorsal root ganglia[42]. These sensory neurons typically project to NTS, from which the information is transmitted to paraventricular nucleus of the hypothalamus (PVN) [43]. PVN, in turn, is believed to pass the information to ACC, insular, and prefrontal cortex[43]. Such ascending circuitry has been proposed to modulate learned fear[44], anxiety-like behavior[45] or sleep[46]. However, whether and how the descending regulation of the heart and the ascending feedback from the heart might drive the heart-behavior coupling remains unknown.

Drosophila possesses the heart which is an evolutionarily conserved organ that develops through conserved master regulators such as *tinman*, *Nkx2.5* and *GATA*[47–50]. Drosophila heart is comprised of two rows of cardiomyocytes, forming a tubular structure (thus called as the “heart tube”) that runs through the midline of the dorsal side of the abdomen, and is anatomically divided into 4 chambers[51,52]. Like mammalian heart, Drosophila heart receives rich neuronal projections throughout[53,54]. Interestingly, a recent paper reported that visual threat decelerates the heartbeat in Drosophila[55], suggesting the existence of the neuronal mechanism that links the processing in the

brain to the heart. However, how the brain regulates the heart, nor the existence of feedback from the heart that modulates behavior, remains elusive.

We have recently reported that a train of air puffs elicit hyperactivity, avoidance of puffs, and aversion from an otherwise neutral visual object, suggesting that air puffs serve as mechanical threat[56]. Capitalizing on this work, we established an experimental paradigm to assess how mechanical threat modulates the heartbeat and behavior in an orchestrated fashion, and set out to elucidate the mechanism that couples cardiac and behavioral threat responses.

RESULTS

I. Air puffs induce cardiac deceleration and locomotion

We have previously reported that a train of air puffs serve as mechanical threats, eliciting a host of fear-like behaviors such as hyperactivity, avoidance of puffs, and aversion from an otherwise neutral visual object[56]. This motivated us to test how the air puff might influence heartbeat, and its relation to behavior. For this purpose, we developed a paradigm to monitor heartbeat and behavior simultaneously (Fig. 1a). Our paradigm images the heart chamber closest to the thorax, called conical chamber, which is visualized through the dorsal cuticle by cuticle-penetrating infare-red light (Fig. 1a, "CAM1"). Simultaneously, the fly's behavior is recorded from the side of the fly (Fig. 1a, "CAM2"). We further developed a set of software to automatically detect heartbeat and behavior (Supplementary Movie 1). Our heartbeat detection software takes two consecutive frames and calculates for each pixel the optical flow, which are used to quantify the overall relaxation (diastole) or shrinkage (systole) of the heart (Supplementary Fig. 1a-c). Based on such quantification, our software detects the timings at which the heart was shrunk most (systole peak), which were counted to obtain the heart rate (HR). Our analysis pipeline for behavior detection first tracks the coordinate of body parts (joints of each leg, eye, neck, haltere, rostral tip of the abdomen, all on the right side of the fly), utilizing SLEAP software[57]. The tracked coordinates are then fed into our custom support vector machine-based program to detect locomotion. Our analysis pipeline allowed us to visualize the HR and locomotion over time in a synchronized fashion.

Using our paradigm, we tested how the air puff might influence the HR and locomotion. Specifically, we applied for each fly a 0.5 s air puff (either 20mL/min, 50mL/min, 200mL/min). We repeated 10 trials for each fly with an inter-puff interval of 90s (Fig. 1b). The results of 10 trials were averaged, as we did not observe noticeable trial effects (Supplementary Fig. 2a, c). We found that the air puff transiently decreased the HR (Fig. 1c, d; Supplementary Fig. 2a, b; Supplementary Movie 1). Similar tendency was observed but was statistically insignificant for the strongest puff (200mL/min), which is likely due to the following cardiac acceleration (Fig. 1d). Surgical removal of body parts and silencing experiments of external sensilla or chordotonal organ[58,59] suggest that hair plate neurons and chordotonal organs are at least partially indispensable for puff-induced cardiac deceleration (Supplementary Fig. 3). We also found that the air puff persistently increased the % flies walking, in line with previous reports (Fig. 1e; Supplementary Fig. 2c, d)[56,60]. Thus, our data revealed that the air puff induces cardiac deceleration and locomotion (Fig. 1f), which promoted us to look for neurons responsible for cardiac deceleration.

II. Dopaminergic system is responsible for puff-induced cardiac deceleration

To aid in identifying neurons responsible for cardiac deceleration, we developed yet another paradigm to quantify the HR with higher throughput. In this paradigm, we drove the expression of GFP in the cardiomyocytes using the enhancer of the Hand gene[48], to aid in heartbeat imaging (Fig. 2a, b). GFP signals in pericardiocytes (also known as nephrocytes) are likely due to their function to incorporate any molecules in the hemolymph[61]. The fly's ventral side of the thorax and abdomen were glued to a

slide glass, and the GFP signals in the conical chamber were acquired through the intact dorsal cuticle by confocal microscopy (Fig. 2a, b). The air puffs of 20mL/min were applied frontally to the fly's head through a glass pipette (Fig. 2a). Heartbeat was detected using our custom software (Supplementary Fig. 4a-c). A single trial consisted of 60 s of interval, 10 s of air puffs, and 60 s of recording, which was repeated twice for each fly with 90s interval (Fig. 2c). This experiment revealed that air puffs induce cardiac deceleration by roughly 10% (Fig. 2d-f; Supplementary Movie 2), consistent with our earlier finding (Fig. 1). Similar results were obtained when the air puff was applied for 1s (Supplementary Fig. 4d, e), 20s (Supplementary Fig. 4f, g), and in both sexes (Supplementary Fig. 4h, i).

Monoaminergic systems have repeatedly been implicated in HR regulation across species, including Drosophila[62–71]. We thus wondered whether monoaminergic systems might be involved in puff-induced cardiac deceleration. When we silenced with TNT the neurons expressing either serotonin, octopamine (insect equivalent of norepinephrine), and dopamine, we found that silencing of octopaminergic or dopaminergic neurons significantly suppressed puff-induced cardiac deceleration (Fig. 2g, h; Supplementary Fig. 5a, b). Note, however, that when we expressed in serotonergic neurons the inward-rectifying potassium channel Kir2.1, it did decrease the puff-induced cardiac deceleration (Supplementary Fig. 5c, d), suggesting that serotonergic neurons may also be indispensable for puff-induced cardiac deceleration. In line with this, a *loss-of-function* mutation of a serotonin synthetic enzyme *TrH* also showed decrease in the puff-induced cardiac deceleration (Supplementary Fig. 5e-g).

To further probe the roles of monoaminergic neurons, we next tested whether thermogenetic activation of these neurons can induce cardiac deceleration without air puffs. To this end, we expressed a heat-gated cation channel dTrpA1 in monoaminergic neurons, and shifted the temperature from 21□ to 28□ while monitoring the HR (Fig. 2i). This revealed that, while the HR of cold-blooded Drosophila increased as a function the temperature even in the driver-less control (Fig. 2j, black), such cardiac acceleration was suppressed by activation of dopaminergic neurons (Fig. 2j, blue) but not by octopaminergic neurons (Fig. 2j, gray). On the other hand, activation of serotonergic neurons exaggerated the heat-induced cardiac acceleration (Fig. 2j, red). The average HR during 28□ period indeed revealed that the activation of dopaminergic neurons significantly decreased the HR compared to the driver-less control, while the activation of serotonergic neurons significantly increased the HR (Fig. 2k). Dopaminergic neurons are thus the only monoaminergic neurons whose silencing and activation consistently suggest their role in driving cardiac deceleration (Fig. 2g-k). The role of dopaminergic neurons is further reinforced by loss-of-function experiments of dopamine receptors, which revealed that mutations of *Dop1R2* or *Dop2R* significantly decrease the puff-induced cardiac deceleration (Fig. 2l, m; Supplementary Fig. 5h, i). A mutation of *DopEcR* also showed a tendency to decrease the puff-induced cardiac deceleration albeit not quite reaching the statistical significance (Fig. 2l, m; Supplementary Fig. 5h, i). Together, our data suggests that dopamine system is responsible for puff-induced cardiac deceleration.

III. Two pairs of dopaminergic neurons in the brain, DA-WED neurons, are indispensable for cardiac deceleration

There are approximately 130 dopaminergic neurons scattered throughout the Drosophila brain[72,73]. To identify the subpopulation of dopaminergic neurons responsible for puff-induced cardiac deceleration, we turned to a host of dopamine-related GAL4 driver lines[72] (Fig. 3a). Each of these drivers carries different bits of enhancers of dopamine-related genes, and presumably for this reason these drivers are known to label partially overlapping but distinct subpopulations of dopaminergic neurons[72]. When we drove the expression of TNT by these drivers, we found that neuronal silencing by 4 out of 10 drivers decreased puff-induced cardiac deceleration (R76F01-, R76F02-, R76F05-, R60F07-GAL4; Fig. 3b, blue plots) without significantly influencing the baseline HR (Supplementary Fig. 6a), suggesting that these drivers label the subset of dopaminergic neurons indispensable for puff-induced cardiac deceleration. Identification of these "hit" drivers allowed us to next employ a split-GAL4 approach to further narrow down the indispensable neurons (Fig. 3c). In the split-GAL4 method, the whole GAL4 protein is split into the DNA-binding domain ("DBD") and the activation domain ("AD"), each fused with a leucine-zipper domain[74]. When these "hemi-drivers" collide, they bind to each other through their respective leucine zipper, re-constituting the functional GAL4. Thus, by placing each of these hemi-drivers under different enhancers, one can achieve the expression of functional GAL4 only in cells in which both enhancers are active (Fig. 3c). When we tested all split combinations of the 4 "hit" enhancers, we found that only one combination, namely R76F05-DBD and R60F07-AD, significantly decreased the puff-induced cardiac deceleration (Fig. 3d), without significantly influencing the baseline HR (Supplementary Fig. 6b). Our immunohistochemical analysis revealed that,

as reported by a previous report[72], the split combination of R76F05-DBD and R60F07-AD labeled two different subpopulations of dopaminergic neurons, called PPL1-SMPγ and DA-WED (Fig. 3e), with additional one or two neurons occasionally labeled in some brains. We further sought to identify which of these two subpopulations is indispensable for puff-induced cardiac deceleration. Taking advantage of the recently-developed analysis pipeline that identify a list of candidate GAL4 drivers that may label any neuron of interest[75,76], we obtained a list of candidate PPL1-SMPγ and DA-WED drivers. By testing several split combinations of enhancers used in these drivers, we could identify the split combinations that label one but not the other (Fig. 3f). We note that each of these combinations labels additional neurons, in either subesophageal zone (Fig. 3f, left) or optic lobes (Fig. 3f, right). Using these split drivers, we silenced either PPL1-SMPγ or DA-WED with TNT, and found that silencing of DA-WED significantly decreased puff-induced cardiac deceleration (Fig. 3g; Supplementary Fig. 6c). Together, our data suggests that DA-WED neurons are indispensable for puff-induced cardiac deceleration.

IV. DA-WED neurons are responsible for puff-induced cardiac deceleration

While our data so far suggests the role of DA-WED neurons in cardiac deceleration, the split driver we used to label DA-WED also labeled neurons in the optic lobes (Fig. 3f; right). We thus further improved the labeling specificity through intersection strategy. In this strategy, the effector gene is expressed under the control of UAS sequence, but a “stop” sequence is inserted in between UAS and GFP, blocking the function of GAL4. Now, the expression of “molecular scissors” called flippase (FLP) is driven by a

Tyrosine hydroxylase (TH) promoter ("TH-FLP"), which excises out the stop sequence. Hence, GAL4 can function only in cells in which TH promoter is active. This strategy, combined with our split GAL4 combination, indeed achieved near-perfect specificity for DA-WED neurons, apparently labeling no other cells throughout the body (Fig. 4a; Supplementary Fig. 6d). When we silenced DA-WED neurons with Kir2.1, it decreased puff-induced cardiac deceleration (Fig. 4b, c), without noticeably influencing the baseline HR (Supplementary Fig. 6e).

We next tested if DA-WED neurons function through dopamine. Our dopamine receptor mutant analysis (Fig. 2l, m) suggests that dopamine signaling through Dop1R2 and Dop2R is indispensable for cardiac deceleration. Consistent with this, we found that RNAi of a dopamine synthesis enzyme ple in DA-WED neurons reduced puff-induced cardiac deceleration (Supplementary Fig. 6f-h). It is thus plausible that DA released from DA-WED neurons binds to Dop1R2 and/or Dop2R to drive cardiac deceleration.

DA-WED neurons have previously been reported to drive protein preference behavior in protein-deprived flies[77,78]. Indeed, suppression of DA-WED neurons decreased protein preference (Supplementary Fig. 7a-d)[77,78] in addition to cardiac deceleration (Supplementary Fig. 7e, Fig.4b, c). This prompted us to ask whether these neurons drive cardiac deceleration and protein preference through shared, or instead distinct, mechanisms. Interestingly, *Dop2R* mutant flies failed to show cardiac deceleration (Fig. 2l, m), but showed normal preference compared to the wildtype (Supplementary Fig. 7f, g). Similarly, suppression of FB-LAL neurons, through which DA-WED neurons drive protein preference[77,78], failed to influence cardiac deceleration (Supplementary Fig. 7h, i). These results suggest that DA-WED neurons drive protein

preference through FB-LAL neurons, while driving cardiac deceleration through Dop2R independent of FB-LAL. This hypothesis is further reinforced by our observations that protein deprivation, which drives protein preference (Supplementary Fig. 7j), fails to influence puff-induced cardiac deceleration (Supplementary Fig. 7k) nor the baseline HR (Supplementary Fig. 7l). Together, our data suggests that DA-WED neurons drive cardiac deceleration and protein preference through distinct mechanisms (Supplementary Fig. 7m).

We next wondered how DA-WED neurons might respond to air puffs. To this end, we expressed jGCaMP7s in DA-WED neurons, and imaged their calcium activities while applying a train of air puffs (Fig. 4d). We found that the calcium level of DA-WED neurons steadily increased as air puffs are applied (Fig. 4e, f; Supplementary Fig. 8a; Supplementary Movie 3). The increased jGCaMP7s signals returned to the baseline in less than 5 s when puffs ceased (Fig. 4f). Given the slow kinetics of jGCaMP7s[79], the increased activity of DA-WED neurons likely returns to the baseline immediately when the puffs cease. While there are two pairs of DA-WED neurons in the brain, one pair being more medial than the other, we found no noticeable difference in medial vs lateral DA-WED neurons' activities in response to puffs (Supplementary Fig. 8b-d). Our data suggests that all four DA-WED neurons transiently get activated by air puffs.

To test if increased activities of DA-WED neurons can replace the air puff to induce cardiac deceleration, we photoactivated DA-WED neurons without puff application (Fig. 4h). For this, we expressed a light-gated cation channel CsChrimson in DA-WED neurons, and shined light on the fly's head to activate these neurons. We found that the photoactivation of DA-WED neurons could induce cardiac deceleration

by ~10% in the retinal-fed test flies, but not in the retinal-unfed control flies (Fig. 4i, j; Supplementary Movie 3).

Together, our data establishes that DA-WED neurons are responsible for puff-induced cardiac deceleration (Fig. 4k).

V. Cardiac interoception possibly contributes to locomotion

Finally, as cardiac interoception has recently been reported to modulate behavior[44–46], we wondered whether feedback from cardiac deceleration in Drosophila modulates locomotion. To test this hypothesis, we silenced DA-WED neurons to block puff-induced cardiac deceleration, and assessed how it might impact locomotion (Fig. 5a). We found that, in the test flies whose DA-WED neurons were silenced, puff-induced locomotion was markedly suppressed compared to the control flies (Fig. 5b, c). To further test the influence of cardiac deceleration on locomotion, we artificially mimicked puff-induced cardiac deceleration[80] (Fig. 5d). Our strategy is to express a light-gated anion channel GtACR1 in cardiomyocytes, using Hand-GAL4 driver, and shine green light to force the cardiomyocytes into a relaxed state (cardiac diastole). We chose an anion channel over cation channels, as we noticed that puff-induced cardiac deceleration is typically accompanied by elongated inter-beat intervals in diastoles but not systoles (Fig. 1c), thus forced diastoles are likely more naturalistic than forced systoles. As expected, when we shined light transiently (a 28ms pulse; Fig. 5e), the heart briefly stopped beating and stayed in diastole (Fig. 5f; Supplementary Movie 5). Our strategy decreased HR by ~ 10% (Fig. 5g, h), thus quantitatively mimicking puff-/ DA-WED- induced cardiac deceleration (Fig. 1d, Fig 4i, j). Interestingly, optogenetic

cardiac deceleration increased locomotion (Fig. 5i, j). Our data hints that the interoception of cardiac deceleration potentially promotes locomotion (Fig. 5k).

Altogether, the present study identifies a group of dopaminergic neurons in the brain responsible for cardiac threat response, and sheds light on the interplay between cardiac regulation and the resultant interoception in shaping organismal threat responses.

DISCUSSION

Here we have revealed that the air puff to fruit flies induces cardiac deceleration and locomotion (Fig. 1). We further identified two pairs of dopaminergic neurons in the brain, called DA-WED neurons, responsible for puff-induced cardiac deceleration (Fig. 4). Interestingly, silencing DA-WED neurons reduces puff-induced locomotion (Fig. 5a, b). Conversely, optogenetic cardiac deceleration induces locomotion (Fig. 5g-j). Collectively, our data suggests a neuronal mechanism in which a mechanical threat induces cardiac deceleration through dopaminergic neurons in the brain, and uncovers how these neurons couple cardiac and behavioral threat responses possibly by engaging interoception.

Dopaminergic neurons in the brain are responsible for puff-induced cardiac deceleration

The present study identified two pairs of dopaminergic neurons in the brain called DA-WED neurons that are responsible for puff-induced cardiac deceleration. Silencing/

photoactivating DA-WED neurons disrupts/ mimics puff-induced cardiac deceleration, respectively (Fig. 4b, c, h-j). Furthermore, DA-WED neurons exhibit calcium elevation upon air puffs (Fig. 4d-g). Circulatory dopamine has long been known to accelerate the heartbeat across species[81]. Indeed in Drosophila, pharmacological application of DA to the heart in a fillet preparation accelerates the heartbeat[63–66], contrary to our findings. However, the responsible source of circulatory DA or DA receptor, as well as whether DA directly acts on cardiomyocytes or instead through some yet unidentified cells, remain elusive. In mammals, cardiomyocytes *per se* express DA and express DA receptors, hinting at the autocrine mechanism[81]. Furthermore, circulatory DA also increases the levels of epinephrine and norepinephrine, complicating the interpretation of ”DA-induced” cardiac acceleration[82]. Our knock-down experiment of DA synthetic enzyme ple in DA-WED neurons suppressed the puff-induced cardiac deceleration (Supplementary Fig. 6f-h), suggesting that DA secreted from DA-WED neurons are indispensable for puff-induced cardiac deceleration. Notably, neurites of DA-WED neurons never exit the brain, suggesting that DA-WED neurons engage circulation or yet unidentified neuronal circuitry to indirectly modulate the heartbeat. Circulation is unlikely to mediate DA-WED neurons’ function, however, given that the air puff and DA-WED activation both induce cardiac deceleration within a second (Fig. 1, Fig. 4). Interestingly, DA acting as a neuromodulator to drive cardiac deceleration has been documented in mammals by a few literatures, either in the ventral tegmental area (VTA) or lateral habenula (LHb)[83,84]. While the existing literature has overwhelmingly stressed the role of DA as hormone, our findings are possibly pointing to an alternative mode of DA action in heartbeat regulation.

DA-WED neurons orchestrate cardiac and behavioral threat responses, potentially by engaging cardiac interoception

Across species, threatening stimulation elicits cardiac and behavioral responses in an orchestrated fashion. Cardiac interoception is postulated to serve as key feedback to link cardiac and behavioral responses[42]. Cardiac interoception is mediated by an array of sensory neurons innervating the heart and aortic arch[42], which convey information to ACC, insular, and prefrontal cortex[43] through brain stem NTS and hypothalamic PVN[43]. Such ascending circuitry has been proposed to modulate learned fear[44], anxiety-like behavior[45] or sleep[46]. Hence the current hypothesis is that the descending regulation of and the ascending feedback from the heart might together drive the heart-behavior coupling, but to date remains untested. Crucially, empirical evaluation of the cardiac regulation of and the feedback from the heart in a single model system has been lacking, making it difficult to assess whether these two mechanisms work in relation to each other or instead just independently. The present study partially fills this knowledge gap, showing that (1) mechanical threat induces cardiac deceleration and locomotion (Fig. 1), (2) DA-WED neurons in the brain are responsible for threat-induced cardiac deceleration (Fig. 4), (3) optogenetic cardiac deceleration promotes locomotion (Fig. 5d-j). Our data points to a scenario in which DA-WED neurons induce cardiac deceleration upon threat, which in turn promotes threat-induced locomotion (Fig. 5k). Our findings thus lend support to the exciting yet largely untested hypothesis that descending and ascending mechanisms work together to orchestrate heartbeat and behavior for survival.

Overall, we have discovered a group of dopaminergic neurons that decelerate the heartbeat following mechanical threat. We further revealed how these neurons regulate both cardiac and behavioral threat responses in an orchestrated fashion, potentially by engaging cardiac interoception. We propose that our findings open up an exciting avenue to the interrogation of how exteroception and interoception couple behavioral and organ threat responses for survival.

ONLINE METHODS

Fly stocks

The following strains were obtained from Bloomington Stock Center (Indiana University): TrH-GAL4 (#38388), Tdc2-GAL4 (#9313), TH-GAL4 (#8848), UAS-TNT (#28838), UAS-Kir2.1::EGFP (#6596), UAS-CsChrimson::mVenus (#55135), UAS-dTrpA1 (#26263), UAS-mCD8::GFP (#32186), UAS-RedStinger (#8547), UAS-IVS-jGCaMP7s (#79032), UAS-GFP RNAi (#41560), UAS-Ple RNAi (#65875), VT046828-AD (#73115), R12D12-DBD (#69213), R48A08-AD (#70707), VT008692-DBD (#86909), empty-AD; empty-DBD (#79603), R70G12-GAL4 (#39552), R38B08-AD (#71032), R81E10-DBD (#68529),VT043775-DBD (#73728), R74C07-GAL4 (#39847), Aes1N-GAL4 (#39847), iav-GAL4 (#52273), R48A07-GAL4 (#50340), UAS-mCherry (#52267), Hand-GAL4 (#48396).

The following strains were obtained from Kyoto Drosophila Stock Center (Kyoto Institute of Technology): Tes1N-GAL4 (#103660).

Hand-GFP was a gift from Dr. Zhe Han (The University of Maryland).

UAS-FRT-stop-FRT-Kir2.1, and UAS-FRT-stop-FRT-CsChrimson::mVenus were gifts from Dr. Barry Dickson (The University of Queensland).

TH-C-GAL4, TH-D-GAL4, TH-F1-GAL4, Vmat-R76F01-GAL4, Vmat-R76F05-GAL4, Ddc-R61H03-GAL4, Ddc-R60F07-GAL4, DAT-R55C10-GAL4, Vmat-R76F01-AD, Vmat-R76F05-AD, Ddc-R60F07-AD, Vmat-R76F01-DBD, Vmat-R76F05-DBD, Ddc-R60F07-DBD, TH-FLP, UAS-FsF-mCD8GFP were gifts from Dr. Mark Wu (Johns Hopkins University).

Dop1R1-attP, *Dop1R2-attP*, *Dop2R-attP*, *DopEcR-attP*, *TrH-attP* were gifts from Dr. Yi Rao (Peking University).

UAS-GtACR1::tdTomato (III) was gift from Dr. Tabata (The University of Tokyo).

Genotypes and sample sizes used in this study are summarized in Supplementary Data 1.

Heartbeat and behavior recording

Flies were maintained on conventional cornmeal-agar-molasses medium under a 9AM:9PM light/ dark cycle at 25 ˚C and 60 +/- 5 % humidity. Flies were collected 0–1 day post eclosion and housed in a group of 9-10 for 2-5 days before testing unless otherwise stated. Male flies were used throughout except for Supplementary Fig. 4h, i, in which both male and female were used. All experiments were carried out between 10 am and 8 pm at 25 +/- 0.8 C and 60 +/- 5 % humidity.

Immediately before the experiments, a fly was briefly (< 1 min) cold anesthetized, and its thorax and abdomen were glued to a glass with a drop of UV bonding glue (Bondic BD-SKCJ) and 405nm UV light (OSV5XME1C1E, Akizuki electronics. Inc). More specifically, for heartbeat recording without behavioral recordings, the ventral side of the fly's thorax and abdomen were glued to a slide glass. For simultaneous recordings of the heartbeat and behavior, the dorsal side of the thorax and abdomen were glued to a coverslip so that the fly can freely walk in our walk simulator.

As for heartbeat recordings without behavioral recording, they consisted of acclimation (10 min) and puff response tests (350s), in this order. A puff response test

consisted of 1 min recording, followed by a train of 10 air puffs (1Hz, totaling 10 s), and then another 1 min recording. For each fly, the puff response test was repeated twice, with the inter-trial interval of 90 s. As for simultaneous recordings of the heartbeat and behavior, they consisted of acclimation (20 min) and puff response tests (950 s), in this order. During puff response tests, an air puff (500 ms) was applied once every 90 s for 10 times. The final puff was followed by 30 s of recording.

Automatic heartbeat detection

To automatically detect individual heartbeats, we developed a set of custom software tools. For infrared (IR)–based heart imaging obtained during simultaneous recordings of cardiac activity and behavior, our heartbeat detection software (Supplementary Fig. 1a) computes the optical flow for each pixel between consecutive video frames. These optical flow measurements are used to quantify global cardiac relaxation (diastole) and contraction (systole). Based on this quantification, the software identifies time points at which cardiac contraction is maximal (systolic peaks), which are then counted to compute heart rate (HR). The precision of the automated detection was evaluated by comparing both absolute HR values and % changes in HR during air-puff stimulation relative to baseline. These analyses demonstrated that the automated method detects absolute HR and stimulus-evoked HR changes with accuracy indistinguishable from manual annotation (Supplementary Fig. 1b, c).

To detect heartbeats in confocal microscopy images of GFP-expressing cardiomyocytes (recorded in the absence of behavioral measurements; Supplementary Fig. 4a), we subtracted each frame from the subsequent frame to compute pixel-wise

differences between consecutive image pairs. This procedure produced positive or negative pixel values in regions surrounding the cardiomyocytes during cardiac contraction (systole) or relaxation (diastole). Specifically, during systole, pixels within the heart tube exhibited positive values corresponding to the current positions of cardiomyocytes, whereas pixels outside the heart tube exhibited negative values corresponding to their previous positions; the opposite pattern was observed during diastole. Systolic and diastolic phases were distinguished by (i) calculating the standard deviation of the positions of positive-value pixels along the axis perpendicular to the heart tube (the y-axis in Supplementary Fig. 4a), denoted as SD(t); (ii) calculating the standard deviation of the positions of negative-value pixels along the same axis, denoted as SD(t–1); and (iii) computing the difference between SD(t) and SD(t–1). Negative values of SD(t) – SD(t–1) indicated systole, whereas positive values indicated diastole (Supplementary Fig. 4a). The precision of the automated detection was evaluated by comparing absolute heart rate (HR) values and % changes in HR during air-puff stimulation relative to baseline. These analyses showed that the algorithm slightly overestimated absolute HR (Supplementary Fig. 4b), but accurately captured stimulus-evoked changes in HR in a manner indistinguishable from manual annotation (Supplementary Fig. 4c).

Automated behavioral identification

To automatically identify behavior on a frame-by-frame basis, videos were analyzed offline using a custom Python-based pipeline. Body-part coordinates—including the joints of each leg, the eye, neck, haltere, and the rostral tip of the abdomen on the right

side of the fly—were tracked using SLEAP software[57]. The tracked coordinates were subsequently transformed to normalize body length and orientation across individuals. Using these standardized coordinates, the speed of each body part was calculated for each pair of consecutive frames. Both the standardized coordinates and corresponding speed measurements were then provided as inputs to a custom support vector machine (SVM)–based classifier, which labeled each frame as “groom,” “walk,” or “halt.” The SVM was trained using the standardized body-part coordinates and speed features as predictors, with manually annotated behavioral labels serving as the dependent variables.

Walk simulator

The fly was fixed on an air-supported foam ball with a diameter of 8 mm (Yuzawaya, Japan) in a sphere holder. The airflow was constantly monitored with a digital flowmeter (MF-FP10N-H06-010, Horiba estec. Inc) and was adjusted to 500 +/- 10 mL/min. The fly and ball were imaged from the right side under 850-nm illumination with a CMOS camera (GE60, Himawari). The heart was imaged from the dorsal side under 850-nm illumination with a CMOS camera (CS135MU, Thorlabs). Imaging of the behavior and the heart were externally triggered by Arduino Uno board at 70 Hz in a synchronized fashion.

Mechanical stimulation

Mechanical stimulation was delivered through a glass pipette (tip diameter of ~2 mm), placed ~2mm in front of the fly, connected with air hose to a compressor (EARTH MAN, Takagi, Japan) via a solenoid valve (EXA-C6-02C-4, CKD). The solenoid valve

was controlled by an Arduino Uno board, which in turn received connection from a desktop computer running the python program which orchestrated the video recordings and puff application. The mechanical stimulation was generated by alternating the solenoid valve between 500 ms-open and 500 ms-closed states (1 Hz). The mechanical stimulation lasted for either 1s, 10s, or 20s, as specified in each figure. The air flow was monitored with a digital flowmeter (MF-FP10N-H06-010, Horiba estec. Inc) and was adjusted to either 20mL, 50 mL, or 200mL/min, as specified in each figure.

Optogenetic activation of DA-WED neurons

Flies expressing CsChrimson, a red-shifted channelrhodopsin variant, in DA-WED neurons were raised on food containing 500 µM all-trans retinal for 2 - 3 days, in the dark, prior to testing. Photoactivation was performed by delivering a 1s LED light pulse (617nm, Thorlabs) to the fly's head. The output for LED was measured with a power meter (S120C and PM120D, Thorlabs) at a position corresponding to the fly's head, and was adjusted to 1 $\mu W/mm^2$. Light stimuli were triggered by python through an Arduino board connected to the LED driver.

Optogenetic cardiac deceleration

Flies expressing GtACR1, a light-gated anion channel, in cardiomyocytes were raised on food containing 500 µM all-trans retinal for 2 - 3 days, in the dark, prior to testing. Photoactivation was performed by delivering a 28ms-long LED light pulse (530nm, Thorlabs) to the fly's heart through the objective lens. The light intensity was adjusted, for each fly prior to the recording, to the minimum intensity required for a light pulse of

roughly 2s to briefly stop the heartbeat. After the recording, the output for LED was measured with a power meter (S120C and PM120D, Thorlabs) at a position corresponding to the fly's heart, and ranged from 9.88 – 21.8μW/mm^2. Light stimuli were triggered by python through an Arduino board connected to the LED driver.

Immunohistochemistry

The following antibodies were used: mouse nc82 (1:10 Developmental Studies Hybridoma Bank), goat anti-mouse Alexa 633 (1:100, Molecular Probe #A21050). Whole brain immunohistochemistry was performed as described previously[85,86]. Briefly, brains were dissected out in 0.3 % PBST, and were fixed in 2 % paraformaldehyde/ PBS for 90 min at room temperature. Brains were then washed in 0.3 % PBST, for > 3 h, and were blocked in 10 % normal goat serum/ 0.3 % PBST for 30 min. Brains were incubated in the primary antibodies in 10% normal goat serum/ 0.3% PBST at 4 ˚C for 2 days. Brains were then washed in 0.3 % PBST for > 5 h, and were blocked in 10 % normal goat serum/ 0.3 % PBST for 30 min. Brains were then incubated in the secondary antibodies in 10 % normal goat serum/ 0.3 % PBST at 4 for 2 days. Afterward, brains were washed in 0.3 % PBST for > 5 h, and incubated in 50 % glycerol/ 0.3 % PBST for 2 h at 4 ˚C. Lastly, brains were mounted on slide glass in Vectashield (Vector Laboratories). Images were taken with Leica TCS SP8 confocal microscope, and processed in ImageJ (NIH) software.

Calcium imaging

Two-photon calcium imaging was conducted as described previously[56] with a few modifications. Two-photon microscopy (Bergamo II, Thorlabs) with a 16x objective lens (16x CFI LWP Plan Flour Objective, Nikon) and with near-infrared excitation (930 nm, Mai Tai 2, SpectraPhysics. Inc., Mountain View, CA) was used. Cuticle of the top of the flies' head and the fat and trachea beneath it were surgically removed. The exposed brain was submerged in saline solution. The extracellular saline had the following composition (in mM): 103 NaCl, 3 KCl, 5 HEPES, 10 trehalose, 10 glucose, 7 sucrose, 26 $NaHCO_3$, 1 NaH_2PO_4, 1.5 $CaCl_2$, 4 $MgCl_2$.We identified DA-WED neurons using the baseline fluorescence of GCaMP. Images were acquired from 1 plane at 152 frames per s (160 x 96 pixels, pixel size = 0.388 µm, dwell time = 0.246 µs). During calcium imaging, a large fraction of the fly's body was glued to the holding plate, and part of the fly's eye compounds was covered with the holder, and the fly was hung in the air. Each fly underwent the sequence of stimuli per fly once or twice, to scan DA-WED neurons on both hemispheres whenever possible. The time courses of $\Delta F/F_0$ were calculated by, for each bin, taking the percent difference from F 10s prior to the onset of the initial puff application (t = -10 through 0s in Fig. 4f).

Surgery

In search of sensory organs indispensable for air puffs to induce cardiac deceleration, halteres, wings, legs, and a3 segments of the antennae were surgically removed using a pair of forceps on ice just prior to testing. Flies that underwent cold anesthesia just prior to testing served as controls.

Feeding preference test

Two days post eclosion male flies were protein deprived by maintaining on 200 mM sucrose (vials with a kimwipe soaked with 2mL of sucrose solution) for 8 days (kimwipe is exchanged every other day). Prep 7.5% yeast and 200mM sucrose in 0.9% of agar, color-labeled with either blue (brilliant blue FCF) or red (sulforhodamine B) tasteless food dyes. The two types of food mix, 1mL each, were then aliquoted into 35mm petri dish separated by a 5x5x35mm acrylic bar into two chambers. A group of 70 flies starved for 3 hours in an empty vial with a kimwipe soaked with 2 mL of water were cold-anesthetized and transferred into petri dish at ZT2 and allowed to feed for 2 hours in the dark. The flies were then killed by transferring the dish to -30C, upside-down, and scored by examining the color of their abdomen. Preference Index (PI) for yeast was calculated as (# flies consuming yeast - # flies consuming sucrose) / (total # flies that fed). Flies with insufficiently colored abdomen were discarded as poorly fed flies.

Data analyses

Data analyses were performed using our custom-written R and python programs.

Statistics

We did not predetermine the sample sizes. The distribution of normality of each group was assessed using Shapiro-Wilk normality test. Parametric tests (unequal variances *t*-test known as Welch's *t*-test or Dunnett's test) were used only when distributions were

deemed normal; otherwise, non-parametric tests were used (Wilcoxon signed rank test, Wilcoxon rank sum test, or Dunn's test). All statistical tests were two-sided. We employed Bonferroni correction to correct for two tests, and correction implemented in Dunnett's or Dunn's test for more than two tests. $p < 0.05$ after corrections for multiple comparison was deemed statistically significant. Neither randomization nor blinding was performed for the group allocation during experiments or data analysis. All box plots are generated so that center line indicates median, box limits indicate upper and lower quartiles, and whiskers indicate 1.5x interquartile range. All the statistical results are summarized in Supplementary Data 2.

DATA AVAILABILITY

Source data for all main text and Supplementary Figures are available via request to the corresponding author.

CODE AVAILABILITY

Source codes used in the current study are available at https://github.com/mtsuji172/heart_behavior.

ACKNOWLEDGEMENTS

We thank T. Katsuki (ThorLabs) for technical support in setting up the hardware; members of the Emoto Lab for advice and support. This study was supported by JSPS (KAKENHI 24K18157), JST (ACT-X JPMJAX242D), Yamaguchi Educational and

Scholarship Foundation to M.T., AMED-CREST (JP21gm310010), Takeda Science Foundation, Torray Foundation, Naito Foundation, and WPI-IRCN to K.E.

AUTHOR CONTRIBUTIONS

M.T. designed the experiments. M.T., J. D., Y. U., and A.O. performed the experiments. M.T. analyzed the data. M.T. and K.E. interpreted the results and wrote the paper.

COMPETING FINANCIAL INTERESTS

The authors declare no competing financial interests.

REFERENCES

1. Hagenaars, M. A., Oitzl, M. & Roelofs, K. Updating freeze: Aligning animal and human research. *Neuroscience and Biobehavioral Reviews* vol. 47 165–176 Preprint at https://doi.org/10.1016/j.neubiorev.2014.07.021 (2014).

2. Babo-Rebelo, M., Richter, C. G. & Tallon-Baudry, C. Neural Responses to Heartbeats in the Default Network Encode the Self in Spontaneous Thoughts. *Journal of Neuroscience* 36, 7829–7840 (2016).

3. Jammal Salameh, L., Bitzenhofer, S. H., Hanganu-Opatz, I. L., Dutschmann, M. & Egger, V. Blood pressure pulsations modulate central neuronal activity via mechanosensitive ion channels. *Science* 383, eadk8511 (2024).

4. Azzalini, D., Buot, A., Palminteri, S. & Tallon-Baudry, C. Responses to heartbeats in ventromedial prefrontal cortex contribute to subjective preference-based decisions. *The Journal of Neuroscience* 41, JN-RM-1932-20 (2021).

5. Ran, C., Boettcher, J. C., Kaye, J. A., Gallori, C. E. & Liberles, S. D. A brainstem map for visceral sensations. 609, (2022).

6. Lang, P. J., Davis, M. & Öhman, A. Fear and anxiety: Animal models and human cognitive psychophysiology. *J Affect Disord* 61, 137–159 (2000).

7. Gordan, R., Gwathmey, J. K. & Xie, L.-H. Autonomic and endocrine control of cardiovascular function. *World J Cardiol* 7, 204 (2015).

8. Koba, S. *et al.* A brainstem monosynaptic excitatory pathway that drives locomotor activities and sympathetic cardiovascular responses. https://doi.org/10.1038/s41467-022-32823-x (2022) doi:10.1038/s41467-022-32823-x.

9. Green, A. L. *et al.* Identifying cardiorespiratory neurocircuitry involved in central command during exercise in humans. *Journal of Physiology* 578, 605–612 (2007).

10. Matsukawa, K. Central command: Control of cardiac sympathetic and vagal efferent nerve activity and the arterial baroreflex during spontaneous motor behaviour in animals. in *Experimental Physiology* vol. 97 20–28 (Blackwell Publishing Ltd, 2012).

11. Yoshimoto, A., Morikawa, S., Kato, E., Takeuchi, H. & Ikegaya, Y. Top-down brain circuits for operant bradycardia. *Science* 384, 1361–1368 (2024).

12. Wink, J. *et al.* Human adult cardiac autonomic innervation: Controversies in anatomical knowledge and relevance for cardiac neuromodulation. *Autonomic Neuroscience: Basic and Clinical* vol. 227 Preprint at https://doi.org/10.1016/j.autneu.2020.102674 (2020).

13. White, D. W. & Raven, P. B. Autonomic neural control of heart rate during dynamic exercise: Revisited. *Journal of Physiology* vol. 592 2491–2500 Preprint at https://doi.org/10.1113/jphysiol.2014.271858 (2014).

14. Rajendran, P. S. *et al.* Identification of peripheral neural circuits that regulate heart rate using optogenetic and viral vector strategies. *Nat Commun* 10, 1–13 (2019).

15. Silvani, A., Calandra-Buonaura, G., Dampney, R. A. L. & Cortelli, P. Brain-heart interactions: Physiology and clinical implications. *Philosophical Transactions of the Royal Society A: Mathematical, Physical and Engineering Sciences* vol. 374 Preprint at https://doi.org/10.1098/rsta.2015.0181 (2016).

16. Prescott, S. L. & Liberles, S. D. Internal senses of the vagus nerve. *Neuron* 110, 579–599 (2022).

17. Veerakumar, A., Yung, A. R., Liu, Y. & Krasnow, M. A. Molecularly defined circuits for cardiovascular and cardiopulmonary control. *Nature 2022* 1–8 (2022) doi:10.1038/s41586-022-04760-8.

18. Pedroni, A. *et al.* Decoding the molecular, cellular, and functional heterogeneity of zebrafish intracardiac nervous system. *Nat Commun* 15, 10483 (2024).

19. Achanta, S. *et al.* A Comprehensive Integrated Anatomical and Molecular Atlas of Rat Intrinsic Cardiac Nervous System. *iScience* 23, 101140 (2020).

20. Armour, J. A. Potential clinical relevance of the 'little brain' on the mammalian heart. *Exp Physiol* 93, 165–176 (2008).

21. Brack, K. E. The heart's 'little brain' controlling cardiac function in the rabbit. *Exp Physiol* 100, 348–353 (2015).

22. Durães Campos, I., Pinto, V., Sousa, N. & Pereira, V. H. A brain within the heart: A review on the intracardiac nervous system. *J Mol Cell Cardiol* 119, 1–9 (2018).

23. Silva, B. A., Gross, C. T., Gräff, J. & Gra, J. The neural circuits of innate fear□: detection , integration , action , and memorization. *Learning and Memory* 23, 544–555 (2016).

24. Headley, D. B., Kanta, V., Kyriazi, P. & Paré, D. Embracing Complexity in Defensive Networks. *Neuron* 103, 189–201 (2019).

25. Gross, C. T. & Canteras, N. S. The many paths to fear. *Nat Rev Neurosci* 13, 651–658 (2012).

26. Kreibig, S. D. Autonomic nervous system activity in emotion: A review. *Biological Psychology* vol. 84 394–421 Preprint at https://doi.org/10.1016/j.biopsycho.2010.03.010 (2010).

27. Battaglia, S. & Thayer, J. F. Functional interplay between central and autonomic nervous systems in human fear conditioning. *Trends Neurosci* 0, (2022).

28. Casto, R., Nguyen, T. & Printz, M. P. Characterization of cardiovascular and behavioral responses to alerting stimuli in rats. *American Journal of Physiology-Regulatory, Integrative and Comparative Physiology* 256, R1121–R1126 (1989).

29. Dielenberg, R. A., Carrive, P. & McGregor, I. S. The cardiovascular and behavioral response to cat odor in rats: unconditioned and conditioned effects. *Brain Res* 897, 228–237 (2001).

30. Signoret-Genest, J. *et al.* Integrated cardio-behavioral responses to threat define defensive states. *Nat Neurosci* 26, (2023).

31. Hashemi, M. M. *et al.* Neural Dynamics of Shooting Decisions and the Switch from Freeze to Fight. *Sci Rep* 9, (2019).

32. Farkas, E., Jansen, A. S. P. & Loewy, A. D. Periaqueductal gray matter input to cardiac-related sympathetic premotor neurons. *Brain Res* 792, 179–192 (1998).

33. Horiuchi, J., McDowall, L. M. & Dampney, R. A. L. DIFFERENTIAL CONTROL OF CARDIAC AND SYMPATHETIC VASOMOTOR ACTIVITY FROM THE DORSOMEDIAL HYPOTHALAMUS. *Clin Exp Pharmacol Physiol* 33, 1265–1268 (2006).

34. Alexander, L. *et al.* Over-activation of primate subgenual cingulate cortex enhances the cardiovascular, behavioral and neural responses to threat. *Nat Commun* 11, 1–14 (2020).

35. Koba, S., Inoue, R. & Watanabe, T. Role played by periaqueductal gray neurons in parasympathetically mediated fear bradycardia in conscious rats. *Physiol Rep* 4, e12831 (2016).

36. Nakamura, K., Nakamura, Y. & Kataoka, N. A hypothalamomedullary network for physiological responses to environmental stresses. *Nature Reviews Neuroscience 2021 23:1* 23, 35–52 (2021).

37. Hermans, E. J., Henckens, M. J. A. G., Roelofs, K. & Fernández, G. Fear bradycardia and activation of the human periaqueductal grey. *Neuroimage* 66, 278–287 (2013).

38. Samuels, B. C., Zaretsky, D. V. & DiMicco, J. A. Tachycardia evoked by disinhibition of the dorsomedial hypothalamus in rats is mediated through medullary raphe. *Journal of Physiology* 538, 941–946 (2002).

39. Rahmouni, K. Cardiovascular Regulation by the Arcuate Nucleus of the Hypothalamus. *Hypertension* 67, 1064–1071 (2016).

40. Li, S. J. *et al.* Melanocortin antagonists define two distinct pathways of cardiovascular control by α- and γ-melanocyte-stimulating hormones. *Journal of Neuroscience* 16, 5182–5188 (1996).

41. Mastrianni, J. A., Palkovits, M. & Kunos, G. Activation of brainstem endorphinergic neurons causes cardiovascular depression and facilitates baroreflex bradycardia. *Neuroscience* 33, 559–566 (1989).

42. Lovelace, J. W., Ma, J. & Augustine, V. ll Defining cardioception□: Heart-brain crosstalk. *Neuron* 1–4 (2024) doi:10.1016/j.neuron.2024.10.009.

43. Shivkumar, K. *et al.* Clinical neurocardiology defining the value of neuroscience-based cardiovascular therapeutics. *Journal of Physiology* 594, 3911–3954 (2016).

44. Klein, A. S., Dolensek, N., Weiand, C. & Gogolla, N. Fear balance is maintained by bodily feedback to the insular cortex in mice. *Science (1979)* 374, 1010–1015 (2021).

45. Hsueh, B. *et al.* Cardiogenic control of affective behavioural state. *Nature* https://doi.org/10.1038/s41586-023-05748-8 (2023) doi:10.1038/s41586-023-05748-8.

46. Yao, Y. *et al.* Cardiovascular baroreflex circuit moonlights in sleep control. *Neuron* 0, (2022).

47. Han, Z., Yi, P., Li, X. & Olson, E. N. Hand, an evolutionarily conserved bHLH transcription factor required for Drosophila cardiogenesis and hematopoiesis. *Development* 133, 1175–1182 (2006).

48. Han, Z. & Olson, E. N. Hand is a direct target of Tinman and GATA factors during Drosophila cardiogenesis and hematopoiesis. *Development* 132, 3525–3536 (2005).

49. Sellin, J., Albrecht, S., Kölsch, V. & Paululat, A. Dynamics of heart differentiation, visualized utilizing heart enhancer elements of the Drosophila melanogaster bHLH transcription factor Hand. *Gene Expression Patterns* 6, 360–375 (2006).

50. Wessells, R. J. & Bodmer, R. Screening assays for heart function mutants in Drosophila. *Biotechniques* 37, 58–66 (2004).

51. Hillyer, J. F. & Pass, G. The Insect Circulatory System: Structure, Function, and Evolution. https://doi.org/10.1146/annurev-ento-011019 (2019) doi:10.1146/annurev-ento-011019.

52. Rotstein, B. & Paululat, A. On the morphology of the drosophila heart. *Journal of Cardiovascular Development and Disease* vol. 3 Preprint at https://doi.org/10.3390/jcdd3020015 (2016).

53. Dulcis, D. & Levine, R. B. Glutamatergic innervation of the heart initiates retrograde contractions in adult Drosophila melanogaster. *Journal of Neuroscience* 25, 271–280 (2005).

54. Dulcis, D. & Levine, R. B. Innervation of the heart of the adult fruit fly, Drosophila melanogaster. *Journal of Comparative Neurology* 465, 560–578 (2003).

55. Barrios, N., Farias, M. & Moita, M. A. Threat induces cardiac and metabolic changes that negatively impact survival in flies. *Current Biology* 0, (2021).

56. Tsuji, M., Nishizuka, Y. & Emoto, K. Threat gates visual aversion via theta activity in Tachykinergic neurons. *Nat Commun* 14, 3987 (2023).

57. Pereira, T. D. *et al.* SLEAP: A deep learning system for multi-animal pose tracking. *Nature Methods 2022 19:4* 19, 486–495 (2022).

58. Tsubouchi, A. *et al.* Topological and modality - specific representation of somatosensory information in the fly brain. *Science* 623, 615–623 (2017).

59. Zhang, N., Guo, L. & Simpson, J. H. Spatial Comparisons of Mechanosensory Information Govern the Grooming Sequence in Drosophila. *Current Biology* 30, 988-1001.e4 (2020).

60. Lebestky, T. *et al.* Two Different Forms of Arousal in Drosophila Are Oppositely Regulated by the Dopamine D1 Receptor Ortholog DopR via Distinct Neural Circuits. *Neuron* 64, 522–536 (2009).

61. Zhang, F., Zhao, Y. & Han, Z. An in vivo functional analysis system for renal gene discovery in Drosophila pericardial nephrocytes. *Journal of the American Society of Nephrology* 24, 191–197 (2013).

62. Keller, N. R. *et al.* Norepinephrine transporter-deficient mice exhibit excessive tachycardia and elevated blood pressure with wakefulness and activity. *Circulation* 110, 1191–1196 (2004).

63. Zornik, E., Paisley, K. & Nichols, R. Neural transmitters and a peptide modulate Drosophila heart rate. *Peptides (N.Y.)* 20, 45–51 (1999).

64. Zhu, Y. C., Yocom, E., Sifers, J., Uradu, H. & Cooper, R. L. Modulatory effects on Drosophila larva hearts: room temperature, acute and chronic cold stress. *J Comp Physiol B* 186, 829–41 (2016).

65. Johnson, E., Ringo, J. & Dowse, H. Modulation of drosophila heartbeat by neurotransmitters. *J Comp Physiol B* 167, 89–97 (1997).

66. Hillyer, J. F. Insect heart rhythmicity is modulated by evolutionarily conserved neuropeptides and neurotransmitters. *Current Opinion in Insect Science* vol. 29 41–48 Preprint at https://doi.org/10.1016/j.cois.2018.06.002 (2018).

67. Majeed, Z. R., Stacy, A. & Cooper, R. L. Pharmacological and genetic identification of serotonin receptor subtypes on Drosophila larval heart and aorta. *J Comp Physiol B* 184, 205–219 (2014).

68. Johnson, E., Sherry, T., Ringo, J. & Dowse, H. Modulation of the cardiac pacemaker of Drosophila: Cellular mechanisms. *J Comp Physiol B* 172, 227–236 (2002).

69. Schroeder, C. & Jordan, J. Norepinephrine transporter function and human cardiovascular disease. *American Journal of Physiology - Heart and Circulatory Physiology* vol. 303 1273–1282 Preprint at https://doi.org/10.1152/ajpheart.00492.2012 (2012).

70. Sujkowski, A., Gretzinger, A., Soave, N., Todi, S. V. & Wessells, R. Alpha- and beta-adrenergic octopamine receptors in muscle and heart are required for Drosophila exercise adaptations. *PLoS Genet* 16, e1008778 (2020).

71. Schiemann, R. *et al.* Identification and In Vivo Characterisation of Cardioactive Peptides in Drosophila melanogaster. *Int J Mol Sci* 20, 2 (2018).

72. Xie, T. *et al.* A Genetic Toolkit for Dissecting Dopamine Circuit Function in Drosophila. *Cell Rep* 23, 652 (2018).

73. Mao, Z. & Davis, R. L. Eight different types of dopaminergic neurons innervate the Drosophila mushroom body neuropil: Anatomical and physiological heterogeneity. *Front Neural Circuits* 3, 612 (2009).

74. Luan, H., Peabody, N. C., Vinson, C. R. R. & White, B. H. Refined Spatial Manipulation of Neuronal Function by Combinatorial Restriction of Transgene Expression. *Neuron* 52, 425–436 (2006).

75. Clements, J. *et al.* NeuronBridge: an intuitive web application for neuronal morphology search across large data sets. *BMC Bioinformatics* 25, 1–25 (2024).

76. Mais, L. *et al.* PatchPerPixMatch for Automated 3d Search of Neuronal Morphologies in Light Microscopy. *bioRxiv* 2021.07.23.453511 (2021).

77. Wu, G. *et al.* Opposing GPCR signaling programs protein intake setpoint in Drosophila. *Cell* https://doi.org/10.1016/j.cell.2024.07.047 (2024) doi:10.1016/j.cell.2024.07.047.

78. Liu, Q. *et al.* Branch-specific plasticity of a bifunctional dopamine circuit encodes protein hunger. *Science* 356, 534–539 (2017).

79. Dana, H. *et al.* High-performance calcium sensors for imaging activity in neuronal populations and microcompartments. *Nat Methods* 16, 649–657 (2019).

80. Men, J. *et al.* Non-invasive red-light optogenetic control of Drosophila cardiac function. *Commun Biol* 3, 336 (2020).

81. Neumann, J., Hofmann, B., Dhein, S. & Gergs, U. Role of Dopamine in the Heart in Health and Disease. *International Journal of Molecular Sciences 2023, Vol. 24, Page 5042* 24, 5042 (2023).

82. Ziegler, M. G., Kennedy, B., Holland, O. B., Murphy, D. & Lake, C. R. The effects of dopamine agonists on human cardiovascular and sympathetic nervous systems. *Int J Clin Pharmacol* 23, 175–9 (1985).

83. Kirouac, G. J. & Pittman, Q. J. A projection from the ventral tegmental area to the periaqueductal gray involved in cardiovascular regulation. *Am J Physiol Regul Integr Comp Physiol* 278, R1643-50 (2000).

84. Sato, Y., Matsumoto, M. & Koganezawa, T. The dopaminergic system mediates the lateral habenula-induced autonomic cardiovascular responses. *Front Physiol* 15, 1496726 (2024).

85. Van Vactor, D. L., Cagan, R. L., Krämer, H. & Zipursky, S. L. Induction in the developing compound eye of Drosophila: Multiple mechanisms restrict R7 induction to a single retinal precursor cell. *Cell* 67, 1145–1155 (1991).

86. Hummel, T. & Zipursky, S. L. Afferent induction of olfactory glomeruli requires N-cadherin. *Neuron* 42, 77–88 (2004).

TABLES

Supplementary Data 1 List of genotypes and sample sizes used in this study

Supplementary Data 2 Statistics of data presented in this study

MOVIES

Supplementary Movie 1 An air puff induces cardiac deceleration and promotes locomotion. A 50mL/min puff is applied in the middle of the movie, as indicated by the red text that appears on the top left panel of the movie. The bottom left panel shows a behavioral recording, with automated body parts tracking (blue dots and lines) superimposed on the raw data. The top right panel shows the raw heartbeat recording, and the bottom right panel shows the pixel-wise, color-coded optical flow (color-to-direction mapping is shown on the top right of the panel). The playback speed is reduced to 0.25 of the original file.

Supplementary Movie 2 A train of 10 air puffs induce cardiac deceleration in a Hand>GFP fly. The playback speed is reduced to 0.25 of the original file.

Supplementary Movie 3 Air puffs activate DA-WED neurons. The left panel shows a schematic of the DA-WED neurons and the actual calcium imaging data (averaged over the total recording), capturing both DA-WED neurons in the right hemisphere. An arrow indicates the neuron shown on the right panel. The right panel shows GCaMP signals at time 0 on the top, and the time-lapse imaging from there during which air puffs were applied.

Supplementary Movie 4 Optogenetic activation of DA-WED neurons induces cardiac deceleration and promotes locomotion. The playback speed is reduced to 0.25 of the original file.

Supplementary Movie 5 Optogenetic cardiac deceleration promotes locomotion. The playback speed is reduced to 0.25 of the original file.

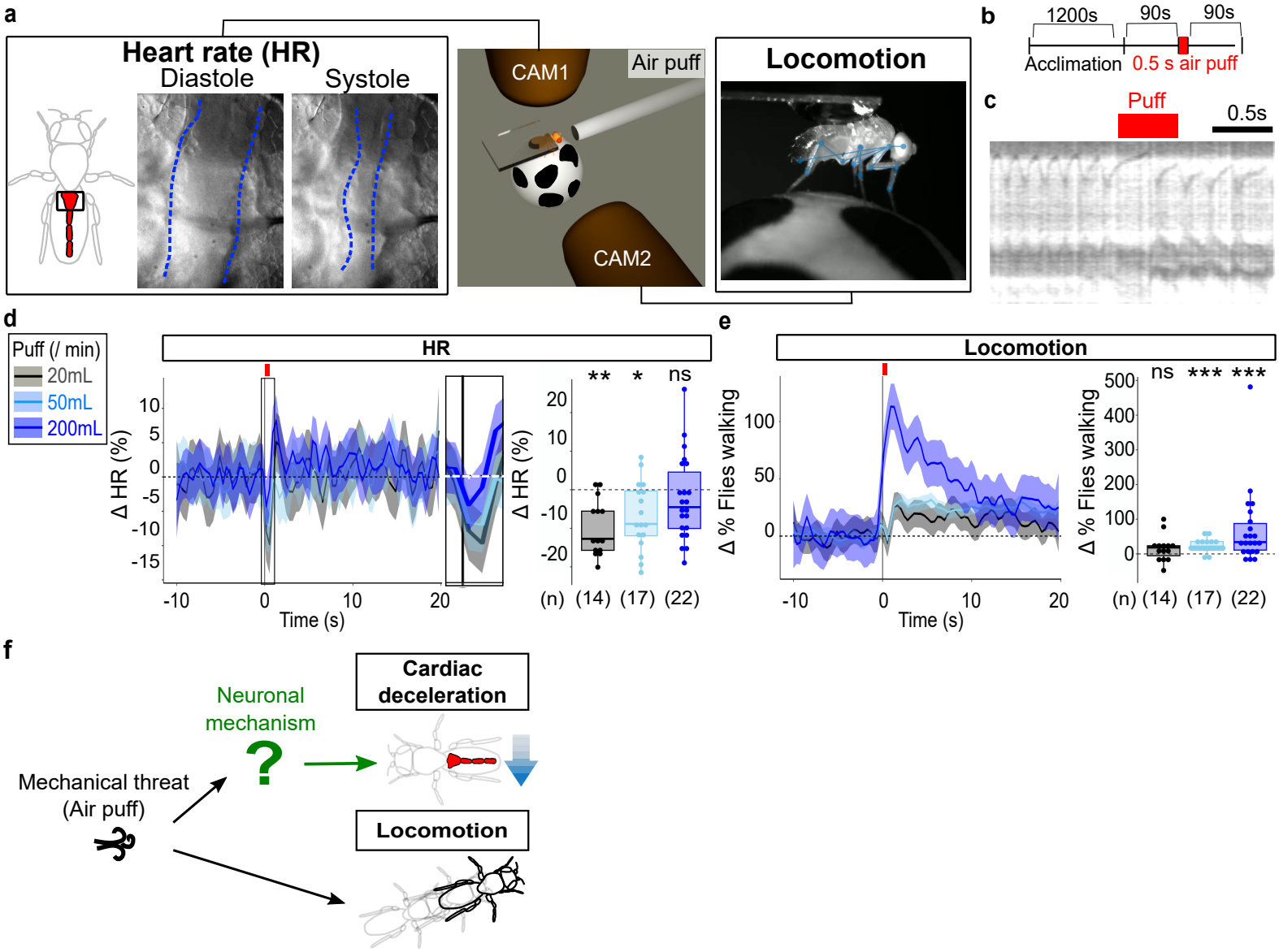

Fig. 1 Mechanical threat induces cardiac deceleration and locomotion

a. Schematics of the paradigm. The fly is fixed on an air-supported ball. Left: the heart rate (HR) was videotaped by an IR-sensitive camera from the dorsal side through the cuticle ("CAM1"). Of the four cardiac chambers, our system videotaped the chamber closest to the thorax called conical chamber. We could easily distinguish diastole and systole in the captured video (blue dashed lines indicate the heart wall). Right: simultaneously, locomotion was videotaped from the right side of the fly ("CAM2"). Blue dots and lines indicate automatically tracked body parts. **b.** The time course of the experiment. An air puffs of 0.5 s was applied once. The trial was repeated 10 times for each fly, the results of which were averaged. **c.** An example M-mode of the heartbeat. An air puff was applied during the red-shaded time window. **d.** Time course of the HR (% change from the average calculated over 10 s preceding the puff onset). N = 14, 17, 22 for 20mL/min (gray), 50mL/min (sky blue), and 200mL/min (dark blue), respectively. **$p < 0.01$, *$p < 0.05$, n.s.: $p > 0.05$, Wilcoxon's signed rank test followed by Bonfferoni correction. The inlet shows the magnified view of the cardiac deceleration indicated by the box. **e.** Time course of % flies walking (% change from the average calculated over 10 s preceding the puff onset). N = 14, 17, 22 for 20mL/min (gray), 50mL/min (sky blue), and 200mL/min (dark blue), respectively. ***$p < 0.001$, n.s.: $p > 0.05$, Wilcoxon's signed rank test followed by Bonfferoni correction. **f.** Model.

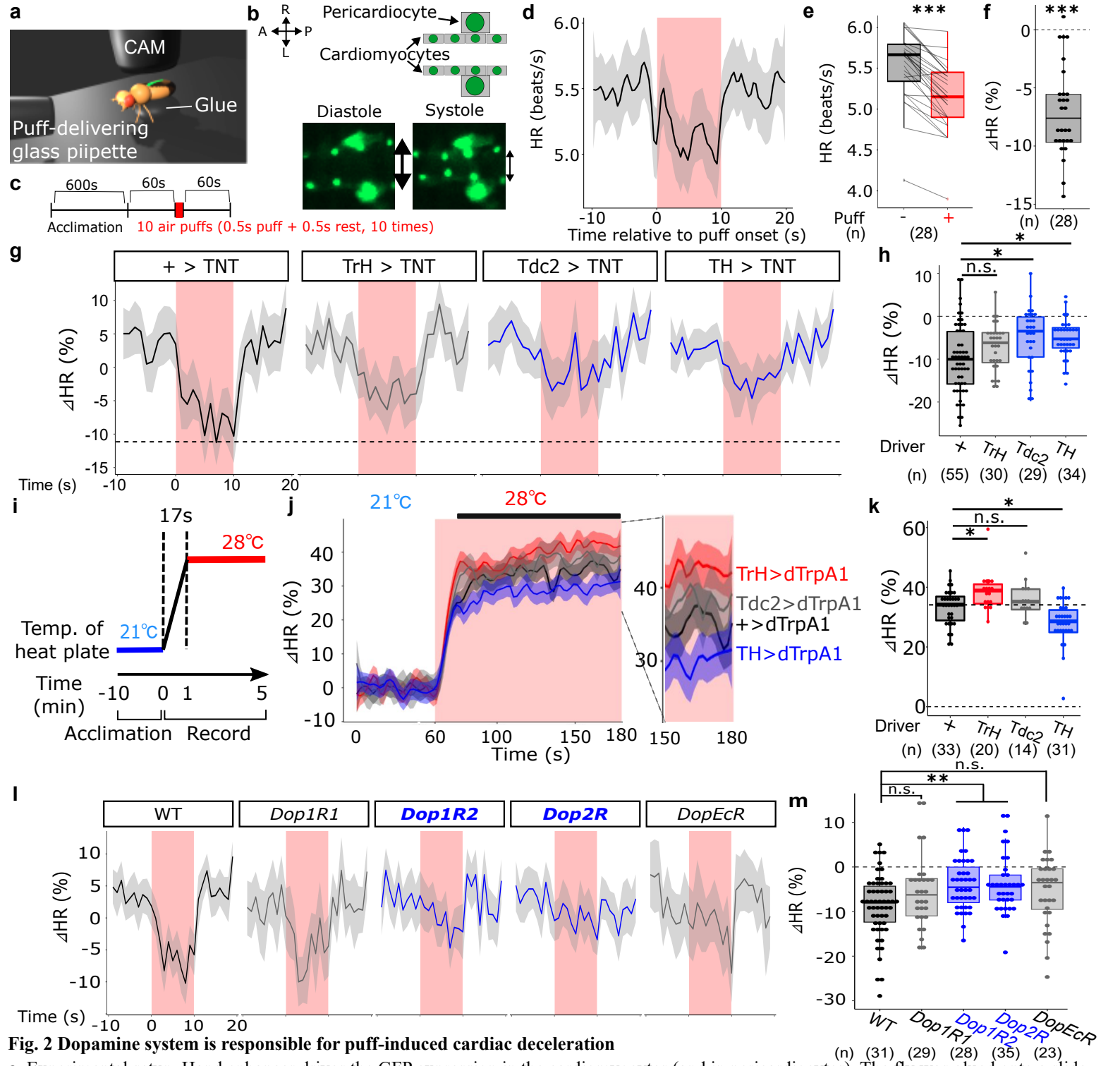

Fig. 2 Dopamine system is responsible for puff-induced cardiac deceleration

a. Experimental setup. Hand enhancer drives the GFP expression in the cardiomyocytes (and in pericardiocytes). The fly was glued onto a slide glass, and the GFP signals were acquired through the intact cuticle. The air puffs were applied frontally to the fly's head. **b.** Example heartbeat. (Upper) Cartoon of the acquired image. Two rows of small cardiomyocytes and one pair of large pericardiocytes are visible. (Lower) Diastole and systole can be distinguished by the changing distance between two rows of cardiomyocytes (arrows). **c.** The time course of the experiment. Air puffs of 0.5 s were applied at 1 Hz for 10 times (totalling 10 s). The trial was repeated twice for each fly, the results of which were averaged. **d.** Time course of the HR. Air puffs are applied during red-shaded window. Lines and shaded areas represent means and SEM, respectively. N = 28. **e.** The HR averaged during puff application window ("puff +") vs 10 s before puff application ("puff -"). Each line corresponds to each fly. N = 28, ***$p < 0.001$, two-tailed *t*-test. **f.** Difference between puff+ HR and puff- HR, calculated for each fly. N = 28, ***$p < 0.001$, two-tailed *t*-test. **g.** Time course of the HR (% change from the average calculated over 10 s preceding the puff onset). Air puffs were applied during the red-shaded time window. Lines and shaded areas represent means and SEM, respectively. TNT expression is driven by indicated drivers. "+" indicates driver-less control. Dashed line shows the lowest mean of "+" control during puffs. N = 55, 30, 29, 34, for +, TrH, Tdc2, TH, respectively. **h.** Difference in the HR averaged over the puff application window ("puff +") vs 10 s before puff application ("puff -"), calculated for each fly. N = 55, 30, 29, 34, for +, TrH, Tdc2, TH, respectively. *$p < 0.05$, n.s.: $p > 0.05$, Dunn's test. **i.** Time course of the experiment. The heat plate beneath the slide glass warmed up the fly. The temperature of the slide glass is held at 21°C for 10 min and ramped up to 28°C for 5min. Note it took approximately 17 s for the temperature to ramp from 21°C to 28°C. **j.** Time course of the HR, shown as % change from HR at 21°C. Temperature was rampted from 21°C to 28°C during red-shaded window. **k.** Changes in the HR (28°C vs 21°C) from the baseline (average over initial 60 s) averaged over 75s - 180s window (shown as black bar in j.). N = 33, 20, 14, 31, for +, TrH, Tdc2, TH, respectively. *$p < 0.05$, n.s.: $p > 0.05$, Dunn's test. The upper dashed line shows the median of "+" control. **l.** The time course of the HR (% change from the average calculated over 10 s preceding the puff onset). Air puffs were applied during the red-shaded time window. Lines and shaded areas represent means and SEM, respectively. N = 31, 29, 28, 35, 23, for +, WT, Dop1R1, Dop1R2, Dop2R, DopEcR, respectively. **m.** Difference in the HR averaged over the puff application window ("puff +") vs 10 s before puff application ("puff -"), calculated for each fly. N = 31, 29, 28, 35, 23, for +, WT, *Dop1R1*, *Dop1R2*, *Dop2R*, *DopEcR*, respectively. **$p < 0.01$, n.s.: $p > 0.05$, Dunn's test.

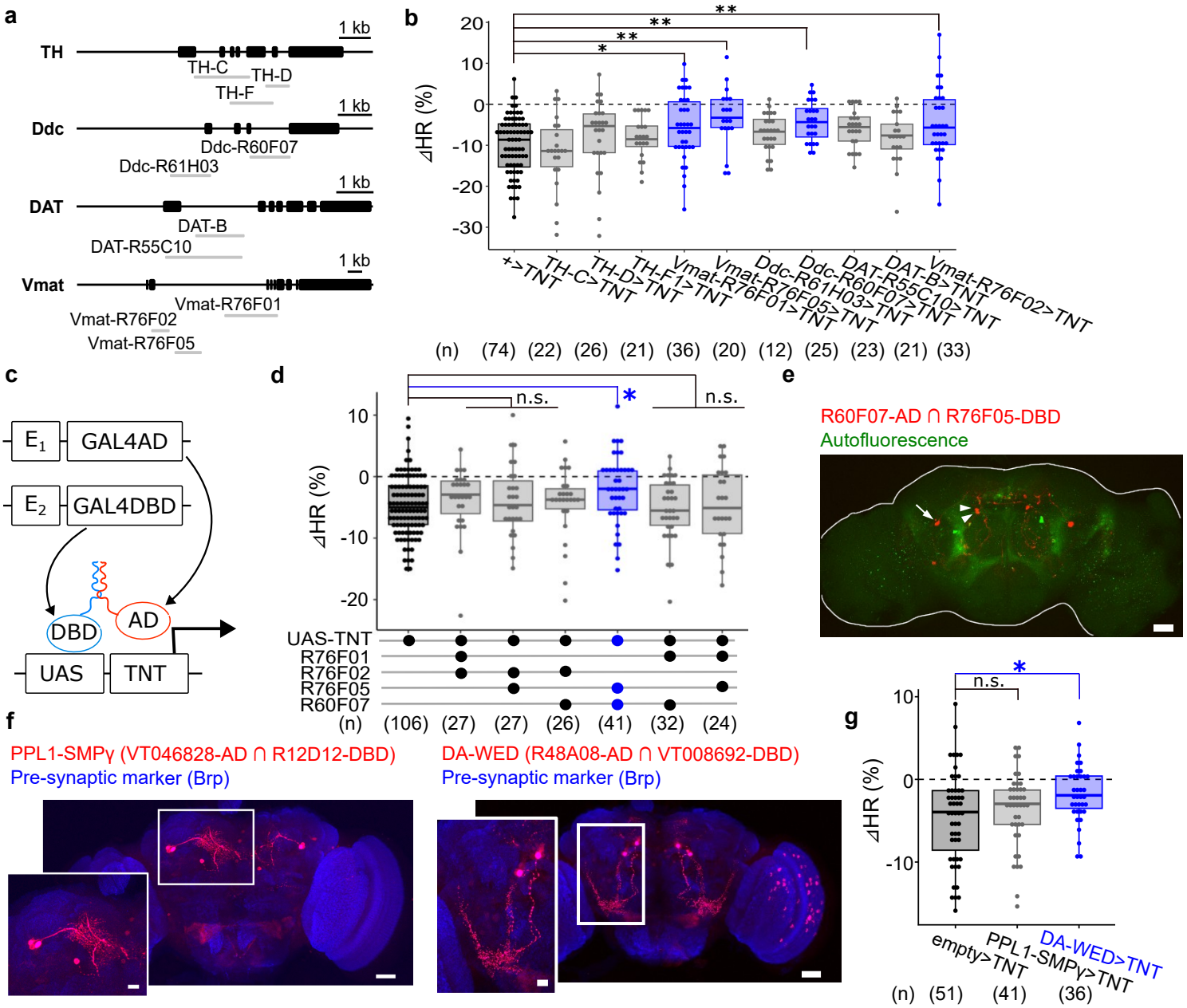

Fig. 3 Two pairs of dopaminergic neurons in the brain are paritally indispensable for cardiac deceleration

a. AsSchematic of different DA-related GAL4 drivers. **b.** Difference in the HR averaged over the puff application window ("puff +") vs 10 s before puff application ("puff -"), calculated for each fly. N = 74, 22, 26, 21, 36, 20, 12, 25, 23, for +, TH-C, TH-D, TH-F1, Vmat-R76F01, Vmat-R76F05, Ddc-R61H03, Ddc-R60F07, DAT-R55C10, respectively. **p < 0.01, *p < 0.05, n.s. (data shown in gray): p > 0.05, Dunnett's test. **c.** A schematic of split-GAL4 strategy. **d.** Difference in the HR averaged over the puff application window ("puff +") vs 10 s before puff application ("puff -"), calculated for each fly. N = 106, 27, 27, 26, 41, 32, 24, for driver-less control, R76F01 ∩ R76F02, R76F02 ∩ R76F05, R76F01 ∩ R76F02, R76F02 ∩ R76F07, R76F05 ∩ R60F07, R76F01 ∩ R60F07, R76F01 ∩ R76F05, respectively. *p < 0.05, n.s.: p > 0.05, Dunn's test. **e.** Brain of R60F07-AD ∩ R76F01-DBD>mCherry (red). An arrow indicates the soma of PPL1-SMPγ, while arrowheads indicate the soma of DA-WED. Scale bar: 25 um. Similar results were obtained across 3 independent samples. **f.** Brains of VT046828-AD ∩ R12D12-DBD>mCherry and R48A08-AD ∩ VT008692-DBD>mCherry (red) immunostained with anti-neuropil marker nc82 (blue). Scale bars: 25 um (inlet: 5 um). Similar results were obtained across 5 independent samples for each genotype. **g.** Difference in the HR averaged over the puff application window ("puff +") vs 10 s before puff application ("puff -"), calculated for each fly. N = 51, 41, 36 for empty>TNT, PPL1-SMPγ>TNT, DA-WED>TNT, respectively. *p < 0.05, n.s.: p > 0.05, Dunnett's test.

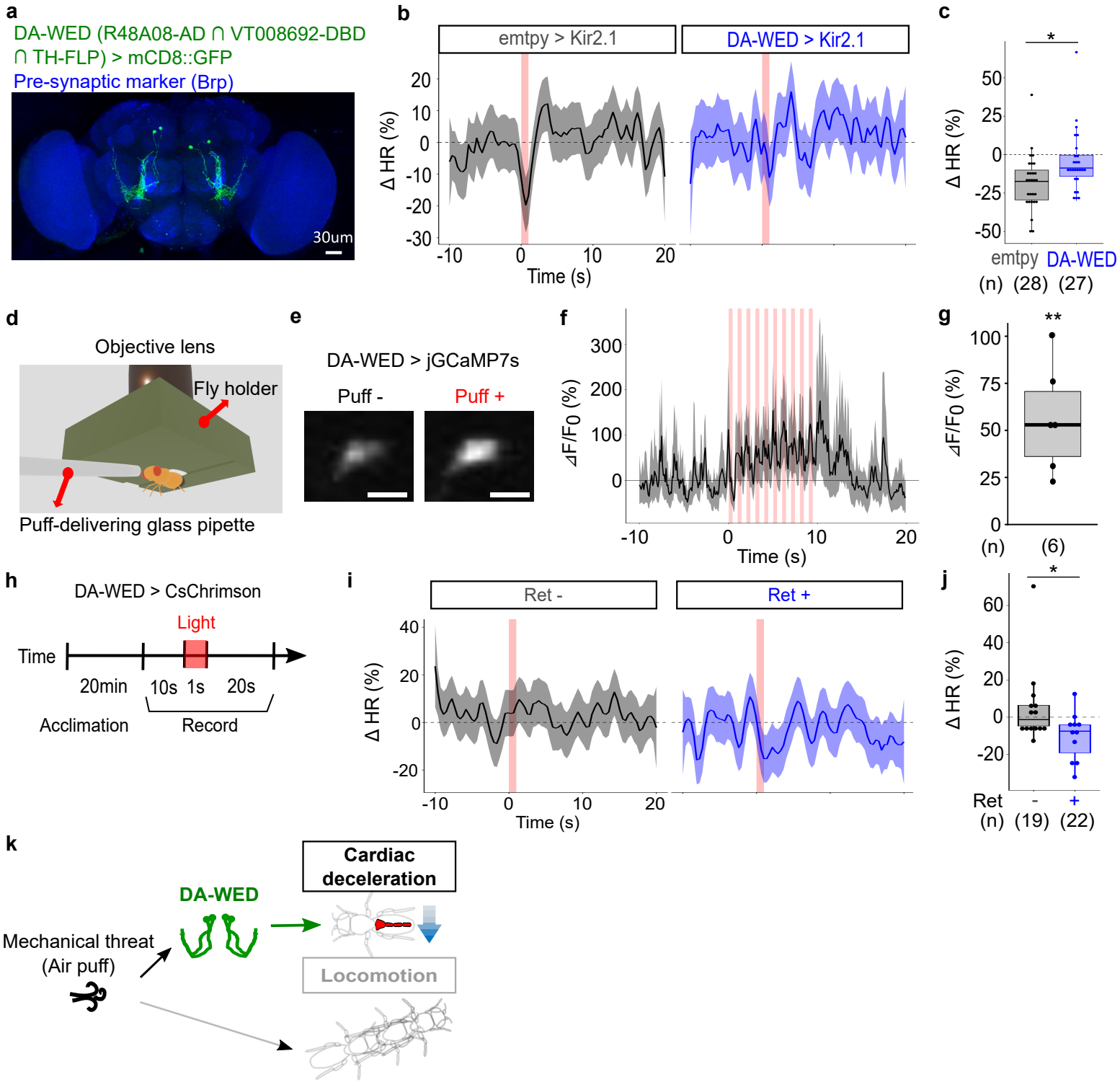

Fig. 4 DA-WED neurons are responsible for puff-induced cardiac deceleration

a. The brain of R48A08-AD ∩ VT008692-DBD ∩ TH-FLP>mCD8::GFP (green) immunostained with anti-neuropil marker nc82 (blue). Scale bar: 30 um. Similar results were obtained across 5 independent samples. **b.** Time course of the HR (% change from the average calculated over 10 s preceding the puff onset). Air puff was applied during the red-shaded time window. Lines and shaded areas represent means and SEM, respectively. N = 28, 27, for empty>Kir2.1, DA-WED>Kir2.1, respectively. **c.** Difference in the HR averaged over the puff application window ("puff +") vs 10 s before puff application ("puff -"), calculated for each fly. N = 28, 27, for empty>Kir2.1, DA-WED>Kir2.1, respectively. *p < 0.05, Two-tailed *t*-test. **d.** Experimental setup. **e.** Representative images of DA-WED neurons expressing GCaMP7s before and during puff application. Scale bar: 5μm. **f.** Time course of $\Delta F/F_0$. Puffs were applied at 1Hz for 10 times (over 10 s), as indicated by red-shaded boxes. N = 6 flies. **g.** $\Delta F/F_0$ averaged over 10s of puff application. When multiple neurons were recorded from the same fly (max 4 neurons per fly), results were averaged so that each dot represents one fly. N = 6 flies. two-tailed *t*-test. **p < 0.01. **h.** Time course of the experiment. After 20 min of acclimation, the heartbeat of the fly expressing light-gated cation channel CsChrimson in DA-WED neurons, with ("Ret +") or without ("Ret -") being fed with the co-factor all-trans retinal (ATR) for 2 days prior to experiment, was recorded for 10s, followed by 1s of light application, and 20s of recording. **i.** Time course of the HR. Red light was shined during the red-shaded time window. Lines and shaded areas represent means and SEM, respectively. N = 19, 22, for Ret-, Ret+, respectively. **j.** Average changes by light shining. N = 19, 22, for Ret-, Ret+, respectively. *p < 0.05, two-tailed *t*-test. **k.** Model.

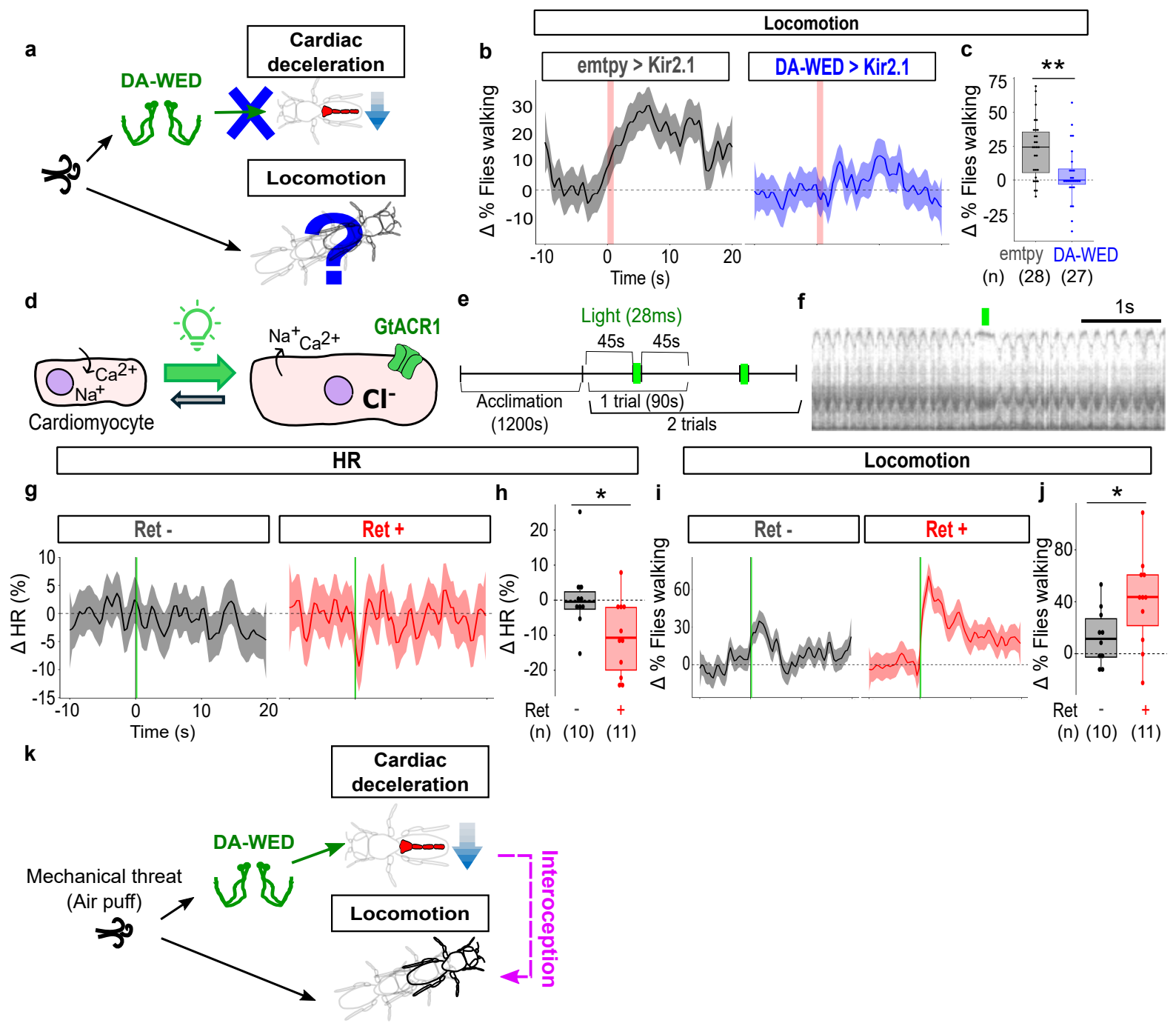

Fig. 5 Cardiac interoception possibly contributes to locomotion

a. The hypothesis. **b.** Time course of % flies walking (change from the average calculated over 10 s preceding the puff onset). An air puff was applied during the red-shaded time window. Lines and shaded areas represent means and SEM, respectively. N = 28, 27, for empty>Kir2.1, DA-WED>Kir2.1, respectively. **c.** Difference in % flies walking averaged over the stimulation window ("puff +") vs 10 s before puff application ("puff -"), calculated for each fly. N = 28, 27, for empty>Kir2.1, DA-WED>Kir2.1, respectively. **$p < 0.01$, Two-tailed *t*-test. **d.** A schematic of the strategy. Cardiomyocytes beat by oscillating between shrunk (systole) and relaxed (diastole) states. Diastole is driven by efflux of cation and resultant hyperpolarization. We expressed a light-gated anion channel GtACR1 in cardiomyocytes using Hand-GAL4, thus artificially driving hyperpolarization by shining light. **e.** Time course of the experiment. After 20 min of acclimation, the heartbeat of the fly expressing GtACR1 in cardiomyocytes, with or without being fed with the co-factor all-trans retinal (ATR) for 2 days prior to experiment, was recorded for 90s, followed by a 28ms light pulse, and 45s of recording. The experiment was repeated twice for each fly. **f.** An example M-mode during optogenetic cardiac deceleration. Green bar indicates when the light was shined. **g.** Time course of the HR (% change from the average calculated over 10 s preceding the light onset). Green light was shined during the breen-shaded time window. Lines and shaded areas represent means and SEM, respectively. N = 10, 11, for ret -, ret +, respectively. **h.** Difference in the HR averaged over the stimulation window ("puff +") vs 10 s before light application ("puff -"), calculated for each fly. N = 10, 11, for ret -, ret +, respectively. *$p < 0.05$, Two-tailed *t*-test. **i.** Time course of the % flies walking (change from the average calculated over 10 s preceding the light onset). Light was shined during the green-shaded time window. Lines and shaded areas represent means and SEM, respectively. N = 10, 11, for ret -, ret +, respectively. **j.** Difference in the % flies walkiing averaged over the stimulation window ("puff +") vs 10 s before light application ("puff -"), calculated for each fly. N = 10, 11, for ret -, ret +, respectively. *$p < 0.05$, two-tailed *t*-test. **k.** Model.